Available online at www.sciencedirect.com
SCIENCE DIRECT®
Journal of Catalysis 225 (2004) 453–465
JOURNAL OF CATALYSIS
www.elsevier.com/locate/jcat

Synthesis of uniform diameter single-wall carbon nanotubes in Co-MCM-41: effects of the catalyst prereduction and nanotube growth temperatures

Yuan Chen, Dragos Ciuparu, Sangyun Lim, Yanhui Yang, Gary L. Haller, and Lisa Pfefferle *

Department of Chemical Engineering, Yale University, New Haven, CT 06520, USA

Received 2 February 2004; revised 20 April 2004; accepted 21 April 2004

Available online 28 May 2004

Abstract

Catalyst pretreatment and CO disproportionation reaction conditions were observed to strongly affect the diameter uniformity of single-wall carbon nanotubes (SWNT) grown on Co-MCM-41 catalysts. The prereduction and CO disproportionation reaction temperatures were varied systematically while the carbon loading and the SWNT diameter uniformity were monitored by TGA, Raman spectroscopy, and TEM. The state of the catalyst during prereduction and the size of the cobalt clusters formed during the SWNT growth process were monitored by in situ XANES during the prereduction of the Co-MCM-41, and ex situ EXAFS of catalyst samples was performed after carbon deposition. These experiments allow development of correlations between the SWNT quality and the state of the catalyst. Control of the cobalt cluster size in the Co-MCM-41 catalyst is critical to the SWNT diameter control. The size of the cobalt cluster changes with both the prereduction and the SWNT synthesis temperatures. SWNT with a very narrow diameter distribution can be grown in Co-MCM-41 by controlling both the prereduction and the reaction temperatures.

Keywords: Cobalt; MCM-41; Single-wall carbon nanotubes; Synthesis; Diameter control

1. Introduction

Many recent experimental studies have been dedicated to the synthesis of single wall carbon nanotubes (SWNT) due to their special electronic and mechanical properties [1–3]. SWNT growth techniques explored so far produce either a broad distribution of tube diameters [4] or SWNT of a narrow diameter distribution at a certain average diameter size imposed by the process used [5,6]. The electronic properties of the SWNT depend on their diameter and chirality. Most electronic applications require SWNT of uniform electronic properties. This requirement may be fulfilled by a synthesis process growing SWNT of uniform diameter and structure. We have recently developed a catalytic system that allows engineered diameter control of the SWNT produced within ±0.05 nm [7]. Mean diameter can be varied over the range from 0.5 to 1 nm. The cobalt catalytic component is incorporated into the pore wall of the MCM-41 mesoporous molecular sieve by isomorphous silicon substitution. During the SWNT growth process, cobalt is reduced and nucleates into metallic clusters that initiate the growth of the carbon nanotubes.

Our previous investigations of SWNT growth by carbon monoxide disproportionation showed SWNT yield, selectivity, and diameter uniformity to be strongly influenced by both catalyst pretreatment and the SWNT growth reaction conditions. Similar observations were previously reported by Resasco's research group working with a different catalytic system consisting of a silica-supported bimetallic cobalt–molybdenum particles [8–10]. The sensitivity of SWNT diameter distribution to growth temperature was also addressed by many other researchers [11–14]. The purpose of the present contribution is to investigate the influence of the process variables on the selectivity and the diameter uniformity of SWNT produced in a monometallic Co-MCM-41 catalyst and how these are affected by the state of the catalyst. This is a first critical step toward the optimization of

* Corresponding author.
E-mail address: lisa.pfefferle@yale.edu (L. Pfefferle).

0021-9517/$ – see front matter
doi:10.1016/j.jcat.2004.04.022

the synthesis conditions. The prereduction and reaction temperatures were varied systematically while monitoring the carbon yield and selectivity, and the diameter uniformity of the SWNT produced. The states of the cobalt catalyst in the MCM-41 material at different stages of pretreatment and reaction were investigated by extended X-ray absorption fine structure (EXAFS), and X-ray absorption near-edge structure (XANES) was carried out in situ during the prereduction step. The ultimate goal is to understand the correlation between the state of the cobalt catalyst and the quality of the SWNT produced.

2. Experimental

2.1. Catalyst

A Co-MCM-41 catalyst with 1 wt% cobalt loading (analyzed by inductively coupled plasma (ICP) at Galbraith Laboratories, Inc.) was prepared following the procedure described in Ref. [15] using a hexadecyltrimethylammonium bromide ($C_{16}H_{33}(CH_3)_2NBr$) as templating material. All reagents used were research grade; the purity of the Cab-O-Sil fumed silica source was 99.8% with chlorine as the only identified impurity (78 ppm). Therefore, cobalt is of very high purity with respect to metals present in our catalyst. The resulting catalyst showed a high structural order with an average pore diameter (by the BJH method [16]) of 2.85 nm and 0.1 nm full width at half-maximum pore size distribution. The pore-size distribution was determined from the nitrogen adsorption-desorption isotherms measured at −196 °C with a static volumetric instrument Autosorb-1C (Quanta Chrome).

2.2. SWNT synthesis

SWNT were synthesized by CO disproportionation. For a typical batch, 200 mg of fresh Co-MCM-41 was loaded into a 10 mm internal diameter quartz reactor placed in an Omega ceramic fiber radiant heater which allows precise temperature control throughout the catalyst bed. Prior to exposure to pure CO (99.5% from Airgas, CO passes through a carbonyl trap to eliminate Fe pentacarbonyl originating from the CO container before entering the reactor) the catalyst was heated in flowing hydrogen at 1 atm at 20 °C/min from room temperature to a desired reduction temperature in the 400 to 700 °C range and reduced isothermally for 30 min. After the prereduction, the catalyst was purged with ultrahigh-purity argon (99.999% from Airgas) at the reduction temperature, and then heated from the reduction temperature to the desired reaction temperature at 20 °C/min in flowing argon. SWNT were grown for 60 min at different temperatures ranging from 650 to 900 °C under 6 atm CO pressure.

2.3. TGA

Thermal gravimetric analysis (TGA) data were collected in a Setaram Setsys 1750 instrument under oxygen flow. Samples were held at 150 °C for 1 h before initiating the temperature program. The weight change in the sample was monitored over the temperature program from 150 to 1000 °C at 10 °C/min for two successive ramps; the second was used as baseline correction for the first. A holey crucible was used to limit mass-transfer interference.

2.4. Raman spectroscopy

Raman spectra of the as-synthesized SWNT without any purification or pretreatment were recorded using an excitation wavelength of 532 nm on a LabRam instrument from Jobin Yvon Horiba equipped with an Olympus confocal microscope. The sample having the narrowest diameter distribution was compared with spectra for multiple excitation wavelength Raman previously reported to confirm these conclusions [7].

2.5. High-resolution transmission electron microscopy (HR-TEM)

HR-TEM images of the fresh Co-MCM-41 and of SWNT were collected on a Tecnai F20 200 kV microscope. The solid samples were dispersed in pure ethanol by sonication and 0.05 ml of this suspension was dropped on a copper mesh coated with an amorphous holey carbon film. The ethanol evaporated prior to the TEM analysis.

2.6. X-ray absorption spectroscopy

All X-ray absorption data were collected at beam line X23A2, National Synchrotron Light Source, Brookhaven National Laboratory. Two 30-cm-long ion chambers filled with pure N_2 were placed collinearly with the beam, in front and behind samples, to measure the incident beams I_0 and transmissive beams I_T. Two types of samples were measured: (i) ex situ samples consisting of Co-MCM-41 samples loaded with carbon after reaction, and (ii) in situ fresh Co-MCM-41 samples during hydrogen reduction. For the ex situ samples, approximately 45 mg of carbon loaded Co-MCM-41 was pressed into a rectangular wafer (ca. 1.5 × 1 cm) to form 0.5-mm-thick pellets. The thickness of pellets satisfied the condition that the absorption edge steps $\Delta\mu x$ at Co K absorption edges are smaller or equal to 1. EXAFS of ex situ samples in transmission mode were recorded from 200 eV below to 1000 eV above the Co K edge. The absorption edge of Co (7709 eV) was determined by placing a Co foil between the ion chambers and this value was used for the edge energy calibration of each sample.

In situ hydrogen reduction experiments were performed at 500 and 700 °C with the fresh Co-MCM-41 catalyst in

order to monitor the state of the catalysts during the hydrogen pretreatment. At the end of these experiments the Co cluster size was determined by EXAFS at room temperature. For the in situ experiments 50 mg of fresh Co-MCM-41 was pressed at ∼5 tons into a round self-supporting wafer (1.5 cm in diameter) using a hydraulic pellet press. Wafers were placed into the stainless-steel reaction chamber, which allowed in situ gas treatment and measurement. The chamber is equipped with beryllium windows (0.5 mm thick), gas inlet, outlet, liquid nitrogen cooling system, and heating elements in the sample holder. The temperature was monitored with a K thermocouple (Omega) placed near the center of the sample holder. Pressure in the chamber was monitored by a pressure gauge (Omega). During the in situ experiment the sample was heated in flowing hydrogen from room temperature to the desired temperature at 20 °C/min and reduced isothermally for 30 min. During this period, XANES data were continuously collected from 30 eV below to 50 eV above Co *K* edge, averaging 5 min per scan, for in situ measurement of the state of the catalyst during reduction. After the in situ reduction, samples were quickly cooled in He flow to room temperature using a liquid nitrogen heat exchanger in the chamber. EXAFS measurements were then performed to assess the size of the Co clusters formed.

3. Results and discussion

The experiments were designed to systematically follow the influence of the pretreatment and synthesis temperatures on the overall carbon yield, and the selectivity and diameter uniformity of the SWNT produced. Cobalt states were investigated before and after reaction and in situ during reduction at two temperatures by EXAFS and XANES. We will further discuss the effect of each investigated process variable in separate sections below.

3.1. Hydrogen pretreatment

SWNT were grown for 60 min with the catalyst heated to 800 °C in argon flow or with hydrogen prereduction at different temperatures, as described in the experimental section. The Raman spectra recorded with the catalysts after SWNT growth as a function of different catalyst pretreatment conditions are given in Fig. 1. Each spectrum was obtained as the average of five spectra recorded at different locations on the same sample. All spectra showed three types of spectral features: the Raman breathing mode peaks at approximately 256 cm^{-1} characteristic for the SWNT, the D band around 1300 cm^{-1} assigned to disordered carbon species, and the peak complex between 1560 and 1600 cm^{-1} known as the G band, which is characteristic for ordered carbon species such as carbon nanotubes and graphite.

The Raman spectrum for the sample without prereduction in Fig. 1 shows several weak peaks in the RBM region suggesting a wide diameter distribution. Most of the low-frequency, weak RBM peaks were less intense when the catalyst was prereduced at 400 °C and were almost completely removed after the catalyst was prereduced at 600 °C. As reduction temperature was further increased to 700 °C, low-frequency RBM peaks corresponding to larger tubes increased again. These results indicate that catalyst prereduction plays a crucial role for the quality of the SWNT grown with this method. The diameter uniformity of the nanotubes grown with the catalyst prereduced at 500 °C was previously demonstrated with multiple excitation wavelength Raman spectroscopy [7]. One sample was also analyzed by fluorescence spectroscopy in the laboratory of professor Weisman at Rice [17]. The florescence spectrum obtained using an excitation wavelength of 671 nm is shown in Fig. 2 along with a graphene map showing the (n, m) tubes identified in the fluorescence experiment, the average diameter observed in TEM experiments, and the largest and smallest diameters predicted by the multiple excitation wavelength Raman experiment described in [7]. Taking into account the RBM upshift by inter-tube or intrabundle interactions as discussed in [13], for the 532-nm laser used in this study, the main RBM peak at 256 cm^{-1} corresponds to tubes with diameter around 0.8–0.9 nm determined by several modified models [18–20], which is consistent with fluorescence, multiple excitation wavelength Raman, and TEM results. These results show that the diameter uniformity of the SWNT samples grown in Co-MCM-41 can be assessed using the 532-nm laser. The wider diameter distribution suggested by the Raman spectra of the SWNT grown without catalyst prereduction was confirmed by TEM. Moreover, the increase in the intensity of the RBM peak at 256 cm^{-1} as the reduction temperature increased from 400 to 600 °C is likely due to the increase of the selectivity for the SWNT identified in fluorescence.

TGA analysis was used to characterize the total carbon loading. Temperature-programmed oxidation was previously used to distinguish among different carbon species in samples [8]. While the amorphous carbon is completely oxidized at temperatures below 350 °C and graphite burns above 750 °C, the oxidation temperature of the SWNT has been observed to vary considerably for samples prepared under different conditions [21,22]. The wide range of the SWNT oxidation temperatures have been attributed to the differences in the catalytic activity of the metallic particles present in the SWNT samples [23]. The presence of tubes both inside and outside the pores of the MCM-41 catalyst may induce oxygen mass-transfer limitations and broaden the distribution of SWNT oxidation temperatures. We only used the TPO data collected in our TGA instrument as a measure of total carbon loading. The total carbon loading is given in Fig. 3 for samples synthesized at different prereduction temperatures. In agreement with the Raman spectra in Fig. 1, the carbon yield increased as the prereduction temperature increased. This behavior is consistent with metallic cobalt clusters initiating the growth of SWNT; more cobalt

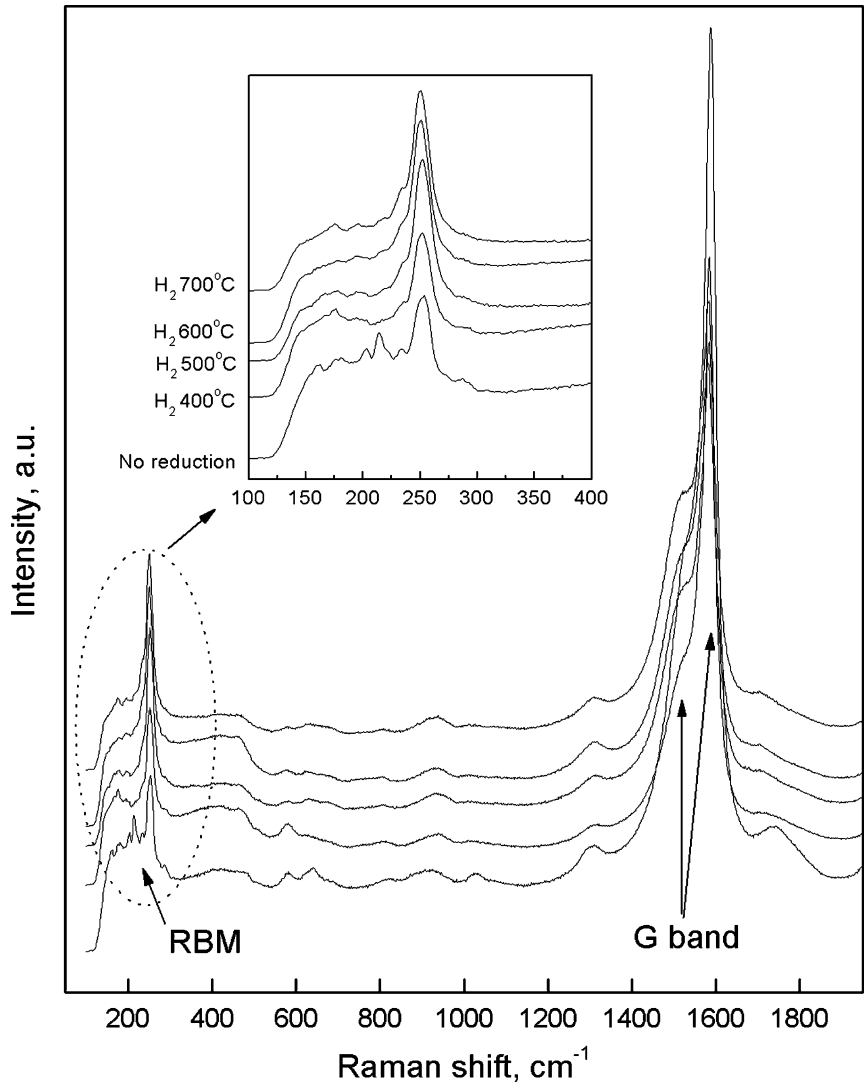

Fig. 1. Raman spectra recorded after SWNT growth with catalyst samples prereduced at different temperatures. The inset shows an enlargement of the Raman breathing mode region.

clusters are generated at higher prereduction temperatures and produce more SWNT. However, as the concentration of metallic cobalt increases in the MCM-41 pores, its nucleation in larger clusters becomes important and SWNT diameter distribution becomes wider.

Whether the metallic cobalt clusters are generated during prereduction or during subsequent exposure to CO is not clear from the experiments described above. Therefore, we employed in situ XANES spectroscopy during hydrogen reduction to investigate the effect of hydrogen pretreatment on the state of the cobalt in the Co-MCM-41. The results of this investigation were then correlated with the carbon yield discussed above.

The normalized in situ XANES data collected during the hydrogen temperature-programmed reduction of Co-MCM-41 are shown in Fig. 4. The temperature program followed the same pretreatment program used for the catalysts prior to SWNT synthesis described above. Two 30-min plateau temperatures were used, 500 and 700 °C, to probe the effect of higher prereduction temperature on the formation of cobalt clusters. XANES spectra were calibrated to the same energy grid using a cobalt foil reference.

Spectra were normalized by FEFFIT [24]. Cobalt foil in the XANES region was also included in Fig. 4 for comparison. The spectral features associated with different cobalt states were observed clearly during the reduction process. First, a preedge peak near 7710 eV related to metallic cobalt was seen to develop as the temperature was increased. After reduction at 500 °C for 30 min, the preedge peak was similar to that observed with the fresh catalyst, suggesting incomplete reduction of Co to the metallic state, while after reduction at 700 °C a clear metallic preedge peak emerged, suggesting the presence of fully reduced metallic cobalt clusters. In addition to the preedge feature, the evolution of the white line at 7725 eV also correlates with the state of the cobalt in the catalyst. The intensity of the white line, which char-

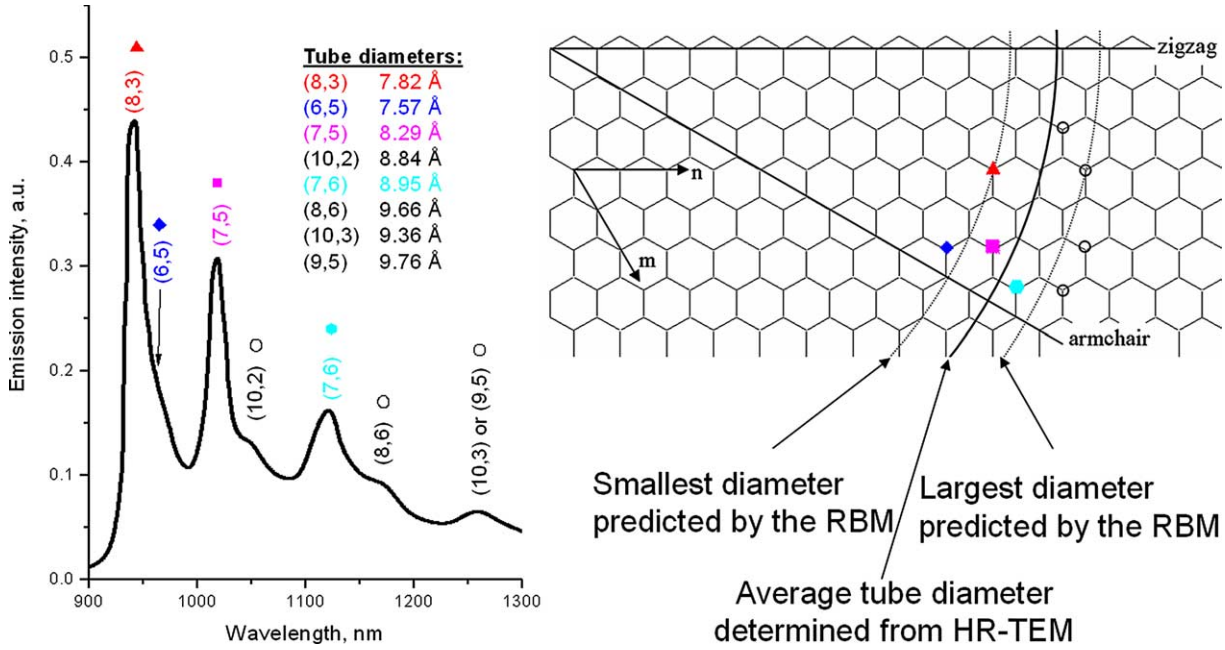

Fig. 2. Fluorescence spectra for a SWNT sample grown in Co-MCM-41 pretreated at 500 °C in H_2 and exposed for 60 min to 6 atm CO at 750 °C. The graphene map shows the tubes identified in fluorescence, the average tube diameter determined by TEM, and the diameter range determined from a multiexcitation wavelength Raman experiment reported elsewhere [7].

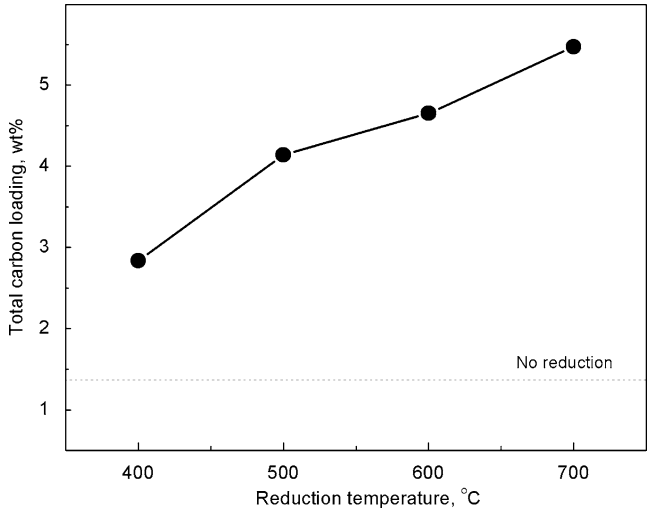

Fig. 3. The carbon yield as a function of the catalyst prereduction temperature.

acterizes cobalt ions, slightly decreased during reduction at 500 °C, suggesting the cobalt is partially reduced by hydrogen at this temperature by removing some of the oxygen from its coordination sphere and creating oxygen vacancies. During reduction for 30 min at 700 °C, however, the intensity of the white line decreased significantly and a preedge spectral feature became apparent, giving evidence for the presence of some completely reduced cobalt clusters. The analysis of the EXAFS spectra recorded at room temperature with the sample prereduced at 700 °C also confirmed the presence of coexisting oxidized and completely reduced cobalt species, with the coordination numbers for the Co–Co and the Co–O shells being 4.86 and 1.73, respectively. The analysis of the EXAFS spectra is discussed in a separate section below.

Fig. 1 shows that SWNT can be synthesized even without catalyst prereduction. However, prereduction increases the carbon yield, suggesting that hydrogen prereduction may be more effective in the extractive reduction of cobalt and/or make the cobalt ions more susceptible to further reduction in a CO environment during SWNT synthesis. This allows more cobalt clusters to form and initiate the growth of SWNT. On the other hand, complete reduction to metal leads to the formation of metallic clusters during the prereduction treatment. These clusters may sinter into larger clusters during heating to the SWNT synthesis temperature, which will grow SWNT of larger diameters with a broader diameter distribution, consistent with the presence of lower frequency RBM peaks observed in the Raman spectra of the sample prereduced at 700 °C in Fig. 1. The effect of hydrogen reduction temperature on the size and state of cobalt clusters formed on Co-MCM-41 is discussed in more detail elsewhere [25]. From these results it becomes evident that the silica matrix in the Co-MCM-41 impedes rapid cobalt reduction, leading to slow reduction of cobalt and the formation of small cobalt clusters highly selective for SWNT synthesis, consistent with our previous reports [7]. It should be noted here that the silica matrix in the Co-MCM-41 may play a similar role to that of molybdenum in the Co–Mo catalyst, which stabilizes the Co in a cobalt molybdate-like compound [9].

Without hydrogen reduction, cobalt was slowly reduced by CO even at elevated temperatures up to 900 °C, resulting

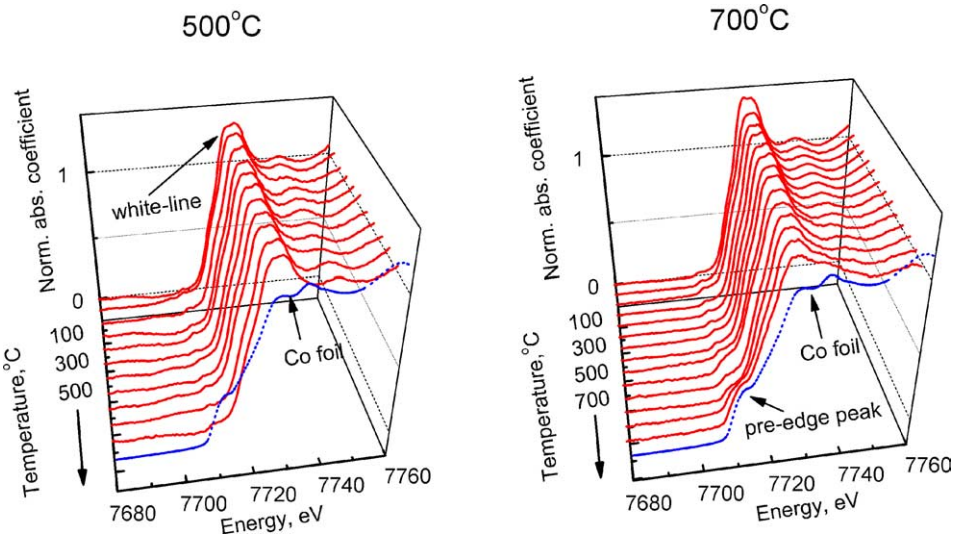

Fig. 4. Normalized XANES spectra near the Co *K* edge recorded during the temperature-programmed reduction of Co-MCM-41 in hydrogen at 500 and 700 °C.

in a weak RBM feature and low carbon loading. When the catalyst is prereduced in hydrogen at too high a temperature (e.g., 900 °C), cobalt aggregates into large particles outside the MCM-41 pores resulting in poor selectivity for SWNT. By controlling the hydrogen prereduction at specified conditions, we can produce partially reduced cobalt and obtain small Co clusters of a narrow size distribution highly selective for SWNT. We have observed that the reducibility of the cobalt is affected by pore size and template synthesis conditions; thus, the optimum prereduction conditions must be determined for each set of synthesis variables.

Prereduction at 500 °C has been used for further investigation of the influence of the SWNT synthesis temperature on the SWNT growth process performance.

3.2. SWNT synthesis temperature

First, the effect of reaction temperature on the quality of SWNT was investigated. Raman spectra recorded for SWNT samples resulting from synthesis at different reaction temperatures are given in Fig. 5. Each spectrum is the average of five spectra recorded at different locations in the same sample. The ratio between the areas of the D and G bands (I_D/I_G) was used as a purity index to qualitatively assess the amount of defective carbon in samples reacted at different temperatures. It should be noted here that this is only a relative assessment as these bands arise from both resonant and nonresonant contributions.

All of the Co-MCM-41 samples were prereduced at 500 °C and reacted for 60 min at 6 atm with pure CO at constant temperatures ranging from 650 to 900 °C. All of these catalysts produced SWNT. From the spectral features in the RBM region in Fig. 5, the Raman spectra of the sample reacted at 650 °C shows many weak peaks over a broad region indicative of a broad diameter distribution. The wide distribution of tube diameters was also evident in TEM

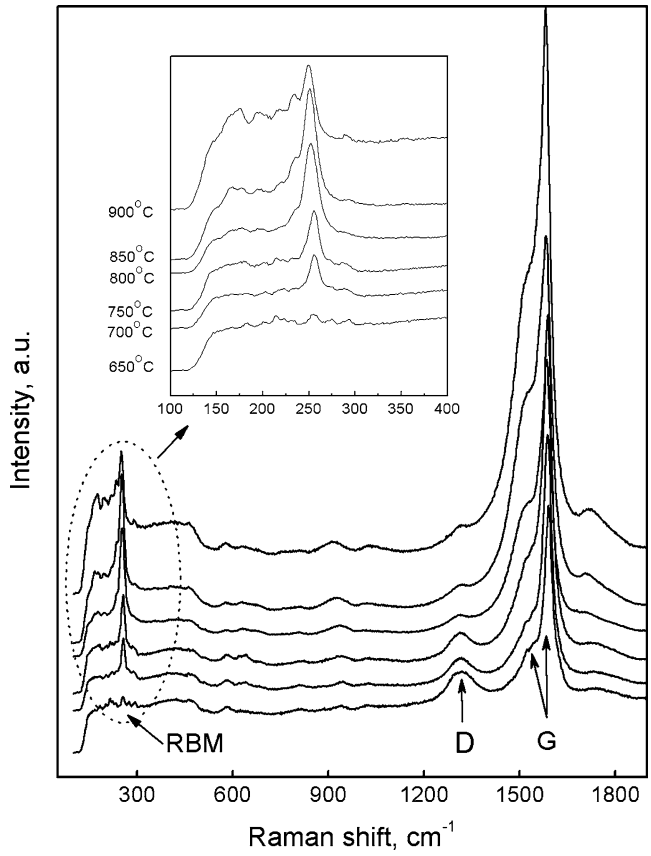

Fig. 5. Raman spectra recorded for catalyst samples after SWNT synthesis at different temperatures using a catalyst pretreated 30 min in hydrogen at 500 °C. The inset shows an enlargement of the Raman breathing mode region.

analysis. As the reaction temperature increases, the peaks in the RBM region become stronger with a narrow, single peak centered at 256 cm^{-1}. The diameter uniformity of the nanotubes suggested by the Raman spectra obtained using the

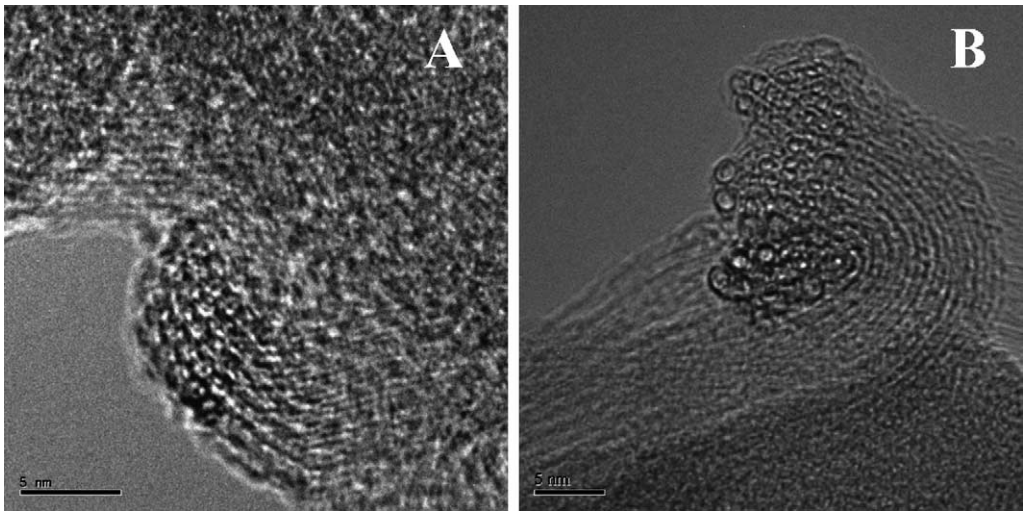

Fig. 6. TEM images showing the diameter distribution of SWNT synthesized at 750 °C (A) and 900 °C (B).

532-nm laser was confirmed by TEM experiments on several grids with specimens grown in different batches under identical experimental conditions, and by a multiple excitation wavelength Raman spectroscopy experiment on one of these samples as reported elsewhere [7]. The diameter distribution becomes broader as the reaction temperatures increases beyond 750 °C, with spectra recorded for the sample obtained after reaction at 900 °C showing several peaks, indicative of SWNT of several diameters. The wide diameter distribution resulting after reaction at 900 °C was also confirmed by TEM; an example of the images is shown in Fig. 6. Note that the SWNT synthesized at 750 °C (micrograph A in Fig. 6) are in a close-packed hexagonal arrangement, characteristic of tubular structures having uniform diameters [26]. By contrast, the tubes imaged in the sample grown at 900 °C (image B in Fig. 6) give evidence of tubes of several different diameters. Observation of several peaks in the RBM region for the SWNT grown with the Co-MCM-41 catalyst is direct evidence that the Raman spectroscopy using the 532-nm laser line is sensitive to the broadening of the diameter distribution of the SWNT in our samples, and can be used as a relative measure of diameter uniformity.

The total carbon loading is shown in Fig. 7 for the samples synthesized at different temperatures, along with the purity index defined above. As the SWNT synthesis temperature increased from 650 to 900 °C, the purity index I_D/I_G decreased from 0.29 to less than 0.01, suggesting the amount of ordered carbon (SWNT or graphite) increased with increasing temperature. The total carbon loading determined by TGA increased from 2.1 to 4.1% when the reaction temperature increased from 650 to 800 °C, then decreased to 2.1% as reaction temperature increased to 900 °C, which indicates a maximum in the carbon yield at approximately 800 °C. Although the decrease of the carbon yield at temperatures higher than 800 °C may convolute the effect of the thermodynamic equilibrium of the CO disproportionation reaction which is disfavored by higher temperatures, these

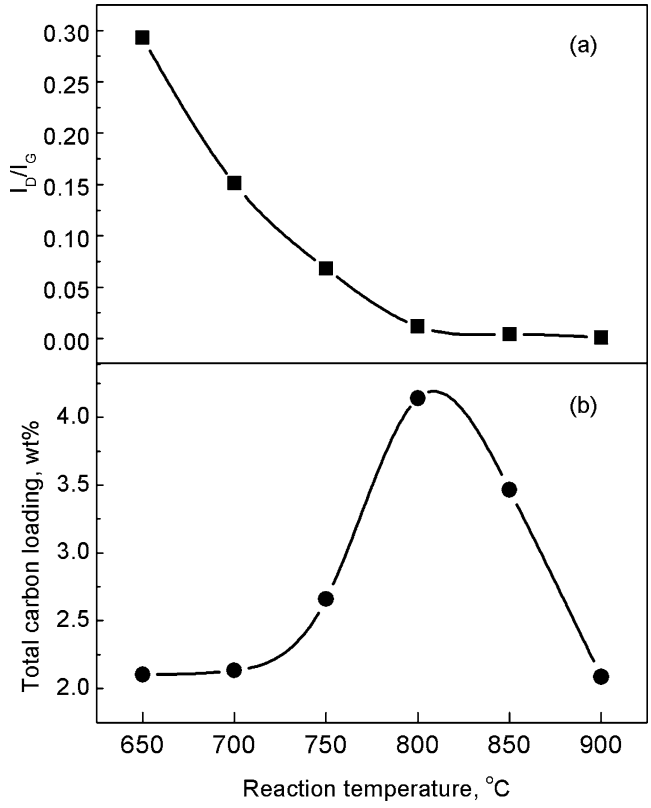

Fig. 7. Variation of the purity I_D/I_G index (a) and of the total carbon yield (b) as functions of the SWNT synthesis temperature.

results suggest that at higher temperatures the Co-MCM-41 is less active for carbon deposition. The temperature corresponding to the maximum carbon yield was observed to increase as the pore size of the MCM-41 template decreases, and this effect is most likely related to the reducibility of the metal in the MCM-41 framework which was observed to decrease as the pore size decreases [25].

A broader distribution of SWNT diameter, as determined by Raman spectroscopy using the 532-nm laser excita-

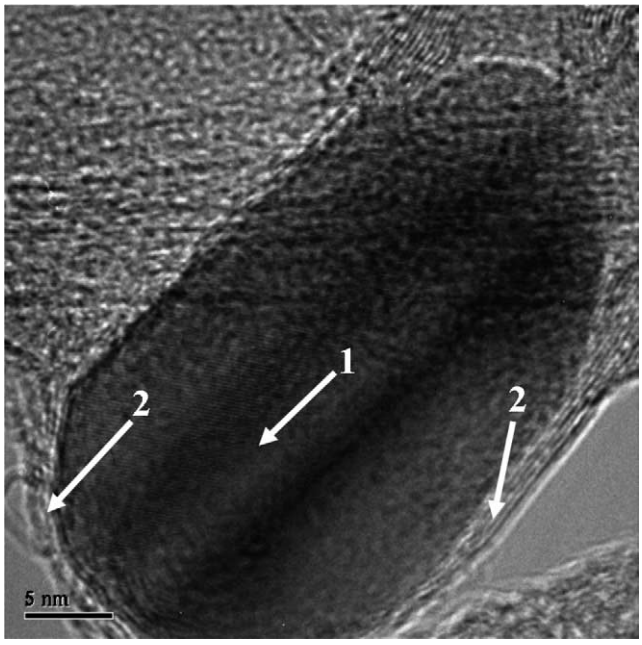

Fig. 8. Transmission electron micrograph showing a large cobalt particle formed during reaction at 900 °C and covered with a continuous layer of carbon. Arrows indicate the lattice spacing of the Co particle (1) and the continuous carbon layer covering the Co particle (2).

tion wavelength, was previously reported by Resasco and co-workers for SWNT samples grown at higher temperatures [27]. However, when compared to the Co–Mo catalyst, the Co-MCM-41 catalyst behaves differently with respect to the carbon yield observed in the same temperature range. The carbon yield obtained with the Co–Mo catalyst decreases as the SWNT growth temperature increases from 600 to 800 °C [28]. The authors explained the decrease of the carbon yield by an increased rate of catalyst deactivation at higher temperatures. The carbon yield observed with the Co-MCM-41 catalyst increased when the temperature increased from 650 to 800 °C and only decreased as the temperature further increased above 800 °C.

Along the lines of the proposed mechanism in which the initially atomically dispersed cobalt ions are partially reduced in the pretreatment stage, and then further reduced to metallic cobalt clusters during SWNT growth, we explain both the low carbon yield and the poor selectivity of the sample reacted at 650 °C by the low number of Co clusters available for SWNT growth. As the reaction temperature increases, the rate of cobalt reduction increases and more cobalt clusters nucleate to reach the optimal size for SWNT growth. This is consistent with the carbon yield increasing as the reaction temperature increases between 650 and 800 °C. However, as the temperature increases, so does the mobility of Co clusters in the MCM-41 pores and the rate of sintering, in agreement with the hypothesis proposed by the Resasco group [27,28]. On the other hand, as a cobalt cluster initiates the growth of a SWNT, it becomes covered with carbon and cannot further sinter into larger metallic clusters. At a certain temperature the rate of cobalt cluster formation surpasses the rate of initiation of the SWNT growth, so that, before the cobalt cluster initiates the growth of a SWNT, it migrates and combines with other Co clusters to give larger metallic clusters, mostly outside the MCM-41 pores. As the size of the cobalt clusters increases, their selectivity for SWNT decreases; they form a surface graphite layer which makes them inactive for CO disproportionation. This is consistent with lower carbon yield at synthesis temperatures higher than 800 °C and more graphite on the surface as the synthesis temperature increases beyond 800 °C. Indeed, the TEM micrograph in Fig. 8 recorded with the sample reacted at 900 °C gives clear evidence of the presence of large cobalt particles covered with graphite. These particles cannot be dissolved in HCl from the SWNT samples removed from the template, likely because the compact graphite layer impedes the access of the acid to the metallic particle. When a prepurified SWNT sample was exposed to microwave radiation, partial oxidation of the covering graphite layer resulted allowing more cobalt to dissolve in a subsequent HCl treatment.

If the proposed mechanism is valid, a slow cobalt reduction process during reaction produces smaller cobalt clusters at lower temperatures, highly selective for SWNT synthesis, and the size of the cobalt clusters should vary with reaction temperature. Such differences in the cobalt clusters size were investigated for samples reacted at different temperatures by EXAFS. The X-ray absorption spectra were analyzed following the procedure described elsewhere [29,30] in four steps. (1) The edge energies were referenced to the edge energy measured with the cobalt foil; background removal and edge-step normalization were performed using the FEFFIT [24]. Full range spectra are shown in Fig. 9. (2) The white line features and the preedge peak details near the Co K edge (7709 eV) were investigated as depicted in Fig. 10. (3) FEFFIT was subsequently used to fit the EXAFS function using paths for metallic and oxidized cobalt species (Co, Co_3O_4) as generated by the FEFF6 program [31]. The fitting was limited to a k range of 2.2–10.0 $Å^{-1}$, k weighted, with modified Hanning windows, $dk = 1.0$ $Å^{-1}$, and an R range from 1.2 to 2.7 Å. The parametric sensitivity analysis performed for different windows, R ranges, and dk values showed that the fitting results were not significantly affected, while the best fittings were obtained with the values given above. The fitting results are plotted in Fig. 11 and the resulting Co–Co and Co–O first shell coordination numbers are given in Table 1 and plotted against the reaction temperature in Fig. 12. (4) The Co–Co first shell coordination numbers were used to estimate the average cobalt clusters size in the Co-MCM-41 catalysts after reaction at different temperatures.

Fig. 9a shows the reaction temperature-dependent normalized absorption coefficient as a function of the scanning energy. Several changes in the EXAFS were observed in this data. The fresh Co-MCM-41 has a strong white line centered at 7725 eV, while the cobalt foil has only a very weak white line. The spectra recorded for samples reacted at dif-

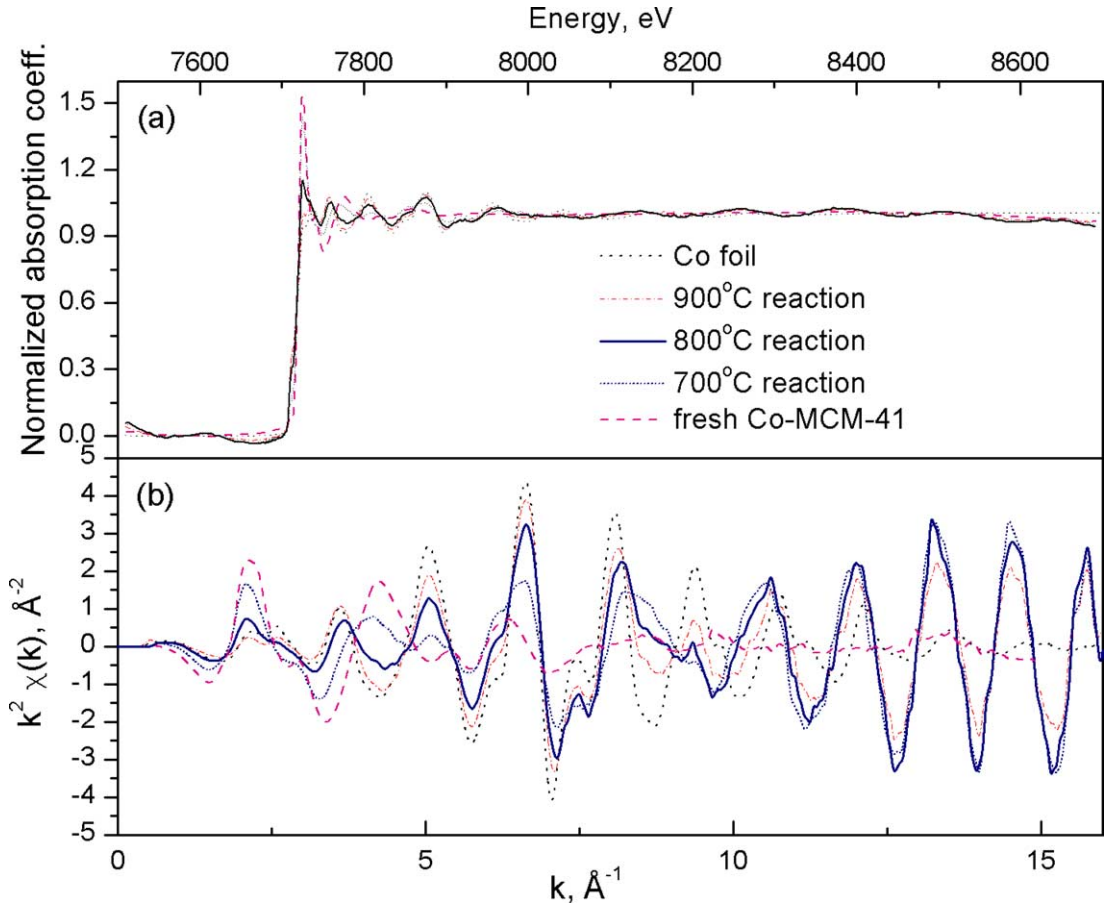

Fig. 9. EXAFS data for Co-MCM-41 catalysts after reaction at different temperatures. The fresh Co-MCM-41 and the cobalt foil are given as references. (a) Normalized EXAFS data calibrated relative to the cobalt foil. (b) The k^2-weighted EXAFS data in the k space.

Table 1
Structure parameters of Co-MCM-41 catalysts from EXAFS fitting

Reaction temperature (°C)	Co–O first shell			Co–Co first shell		
	N_{Co-O}[a]	dR[b] (Å)	σ^2[c]	N_{Co-Co}[d]	dR[b] (Å)	σ^2[c]
700	1.98 ± 0.85	0.14 ± 0.02	0.88	3.46 ± 1.51	−0.05 ± 0.02	1.16
750	1.31 ± 0.60	0.14 ± 0.02	0.89	5.01 ± 1.26	−0.03 ± 0.01	0.83
800	0.73 ± 0.27	0.13 ± 0.01	1.48	7.10 ± 0.87	−0.02 ± 0.01	0.80
850	0.24 ± 0.20	0.12 ± 0.02	1.94	8.62 ± 0.85	−0.02 ± 0.01	0.72
900	0.17 ± 0.20	0.12 ± 0.03	2.15	8.97 ± 1.05	−0.02 ± 0.01	0.71

[a] N_{Co-O} average first shell coordination of cobalt–oxygen.
[b] dR deviation from the effective half-path-length R (R is the interatomic distance for single scattering paths).
[c] σ^2 ($\times 10^{-2}$ Å^2) mean-square deviation in R.
[d] N_{Co-Co} average first shell coordination of cobalt.

ferent temperature were located between the spectrum of the fresh Co-MCM-41 and that of the cobalt foil. The effect of the reaction temperature is also illustrated by the changes in EXAFS amplitude seen across the higher energy range. Fig. 9b shows the same EXFAS data shown in Fig. 9a in a k^2-weighted k space (k is the photoelectron wavenumber). The effect of the reaction temperature is even more clearly presented in k space. The peaks for the cobalt foil (cobalt in a metallic state) and for the fresh Co-MCM-41 (Co in the oxidized state) exhibit different positions and magnitudes in k space. The shifts in the peak position and magnitude are related to both different cobalt states and cluster sizes. The spectrum recorded for the Co-MCM-41 reacted at 900 °C is close to that of the cobalt foil with respect to both position and magnitude, suggesting that cobalt was almost completely reduced after reaction at 900 °C, while the spectra of the Co-MCM-41 reacted at 700 °C is very close to that of the fresh Co-MCM-41, showing that a significant fraction of cobalt is still in the oxidized state after reaction at this lower temperature. The spectrum of the sample reacted at 800 °C

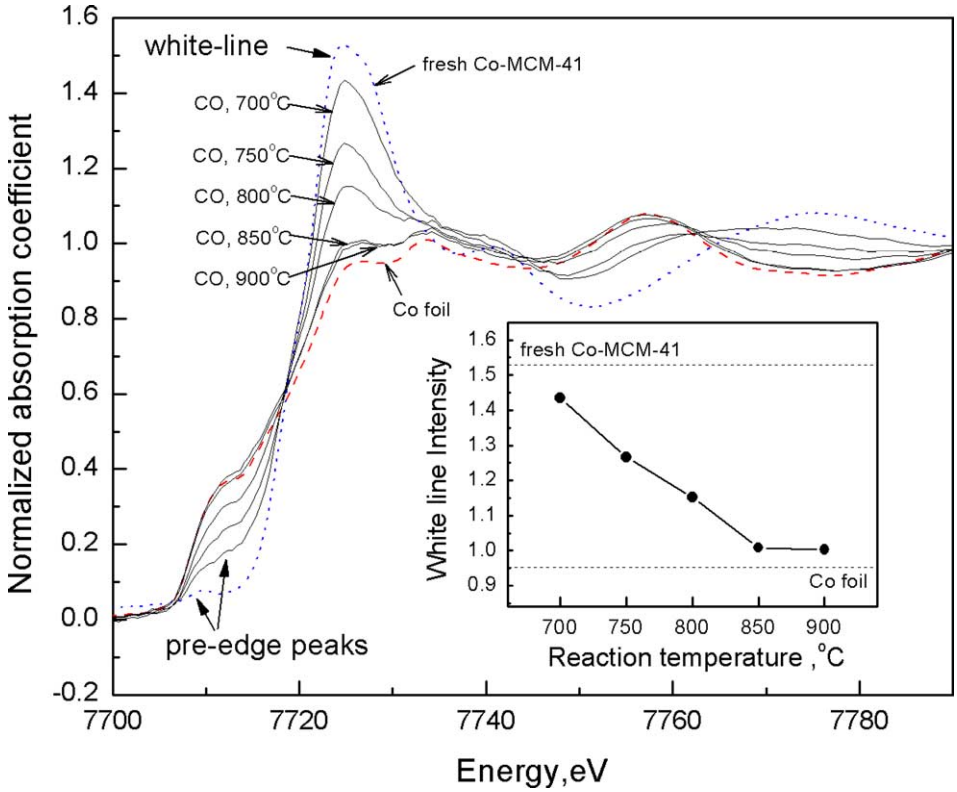

Fig. 10. Normalized EXFAS spectra near Co *K* edge recorded for Co-MCM-41 loaded with carbon after reaction at different temperatures. Spectra for the fresh Co-MCM-41 and cobalt foil are given as references. The inset shows the correlation between the intensity of the white line and the SWNT synthesis temperature.

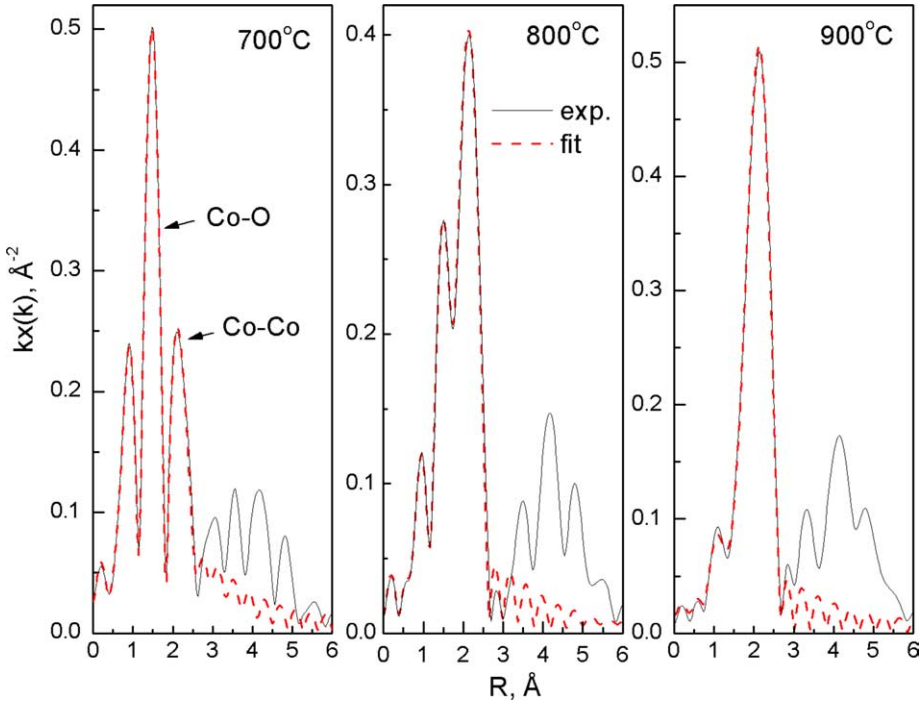

Fig. 11. EXAFS spectra in *R* space for Co-MCM-41 catalysts after reaction at different temperatures along with the fitting of the spectra with theoretical models.

showed, as expected, an intermediate state between those of the samples reacted at 700 and 900 °C.

Fig. 10 illustrates the EXAFS spectra near the Co *K* edge (7709 eV) obtained with Co-MCM-41 samples after reaction at different temperatures. The spectrum recorded with the Co foil reference is also given for comparison. The preedge peaks indicate that cobalt in the fresh Co-MCM-41 is a mixture of Co^{2+} and Co^{3+} in tetrahedral and distorted tetrahedral coordinations with a pseudo-octahedral environment, most likely due to hydration, as discussed elsewhere [15]. The cobalt foil has a strong preedge peak assigned to metallic cobalt. The increase of the preedge feature for the Co-MCM-41 catalyst as the reaction temperature increased constitutes direct evidence for the increase in the cobalt reduction to metallic cobalt as SWNT are synthesized at higher temperatures.

The white line feature is assigned to unfilled d states at the Fermi level. For metals with completely filled d states (e.g., copper) the absorption edge is of the form of a simple step function; the intensity of the white line increases with the number of unfilled d states [32]. The changes in the white-line intensity have been used to characterize the d-hole populations in alloys [33]. For metallic cobalt the presence of 7 electrons in d orbitals gives a weak white line, while for the oxidized cobalt with fewer electrons in d states the white line is stronger. Partial reduction of cobalt in the Co-MCM-41 catalyst during SWNT synthesis was evident from the decrease in the intensity of the white line between the fresh Co-MCM-41 and the completely reduced Co foil observed in Fig. 10. The inset in Fig. 10 shows the variation of the intensity of the white line with the reaction temperature. The spectra of the fresh Co-MCM-41 and of the Co foil have white-line intensities of 1.53 and 0.95, respectively. As the reaction temperature increases from 700 to 900 °C, the intensity of the white line decreased from 1.44 to 1.00, clearly showing different degrees of cobalt reduction for reaction at different temperatures. Higher reaction temperatures cause more cobalt reduction. After reaction at low temperatures (lower than 750 °C), a large fraction of the cobalt remained oxidized, consistent with the lower carbon yield observed in Fig. 7. As the reaction temperature increased above 800 °C, the cobalt was almost quantitatively reduced.

Because in Co-MCM-41 there is a mixture of Co^{2+} and Co^{3+}, there are two different Co–O bonds: a short Co–O bond in Co_2O_3 and a longer Co–O bond in CoO. FEFF6 generated two main Co–O paths from the crystalline structure of Co_3O_4 [34] related to the two different Co–O bond lengths. Using each of these two paths, and both of them simultaneously, to fit the fresh Co-MCM-41 we observed that the path corresponding to the short Co–O bond gave an acceptable fitting for a coordination number of 4, and adding the second path did not significantly improve the fitting. Therefore, we used only two scattering paths to fit the data: the first Co–O path in Co_3O_4 and the first Co–Co path in Co metal. The energy shifts for each shell were observed to have small changes for samples reacted at different temperatures, and thus were subsequently set constant at 5.57 eV for the Co–Co shells and 2.41 eV for the Co–O shells. The passive electron reduction factor (S_0^2) was set to 0.9, as recommended by Rehr and co-workers [35]. Consequently, the fitting was performed having only the coordination numbers and the radial distance of each shell as variables.

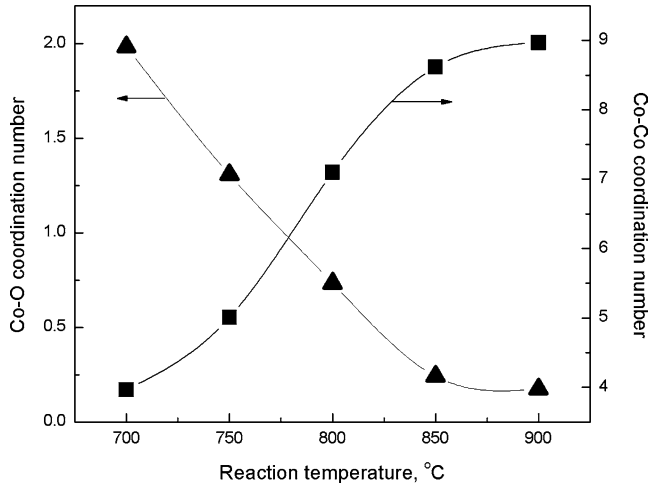

Fig. 12. Coordination numbers of the first Co–O and Co–Co shells as a function of reaction temperature, as fitted from the EXFAS spectra.

The k-weighted EXAFS spectra recorded with the samples after reaction at 700, 800, and 900 °C are shown in Fig. 11 along with the fitting results obtained using the two theoretically calculated paths. There is good overall agreement between the fitting and the experimental data for all samples. The peaks related to the Co–O bond decreased when the reaction temperature increased, most likely because of the higher degree of reduction in the samples reacted at higher temperatures. In contrast, the intensity of the Co–Co peak increased for samples reacted at higher temperatures consistent with a higher degree of Co reduction to metallic clusters. The structural parameters resulting from the fitting using the two paths and their estimated errors are presented in Table 1, and the decrease of Co–O coordination numbers and the increase of Co–Co coordination number with the increase of reaction temperature are illustrated graphically in Fig. 12.

As previously reported, EXAFS has been widely used to determine the size of nanoparticles because of the strong and nonlinear correlation between the particle diameter and the coordination number of atoms in small clusters [7]. We also used the Co–Co first shell coordination number fitted from EXAFS spectra recorded with catalyst samples after reaction at different temperatures to determine the approximate size of the cobalt cluster formed during SWNT growth in an attempt to establish a correlation with the diameter distribution of SWNT produced. We have built a (111)-truncated hemispherical cuboctahedron model to correlate the cobalt cluster diameter with the average first shell coordination number. The variation in the Co coordination number with the cluster size is given by the curve in Fig. 13. Average

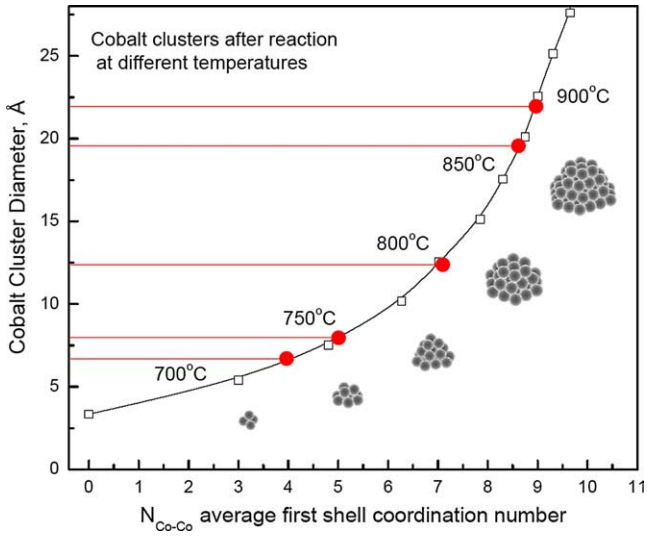

Fig. 13. Variation of the Co–Co coordination number with the first shell with the cluster diameter determined for the cobalt (111)-truncated hemispherical cubic octahedron model. The round gray symbols show the coordination numbers determined from the analysis of the EXAFS spectra.

coordination numbers for cobalt in Co-MCM-41 after reaction are plotted on the theoretical curve along with approximate cluster sizes. The results show the expected increase in cluster size as a function of reaction temperature with a jump between 800 and 850 °C. Correlating these results with the Raman spectra in Fig. 5 provides a direct confirmation of our hypothesis that small cobalt clusters form SWNT of very narrow diameter distribution. However, it is important to note here that, as discussed by Frenkel et al. [30], the geometry of clusters with different sizes, shapes, or lattice symmetries generate different coordination numbers. Although the (111)-truncated hemispherical cuboctahedron model provides a good approximation, the cobalt clusters may have different shapes. In fact, the shapes are likely influenced by ultrasmall particles interacting with the pore wall of the MCM-41 material. These cluster diameters determined by EXAFS only give an average approximation for the cluster sizes. Also, as discussed in [7], the metallic particles formed outside the pore system are more likely to sinter and grow into larger particles than those inside the pores. These larger cobalt particles are likely selective for the growth of graphite and amorphous carbon, depending on the reaction conditions (i.e., higher temperatures produce more graphite, while lower reaction temperature form more amorphous carbon). The EXAFS spectra reported here provide a volume average coordination number which includes larger particles outside the pores. The actual metallic clusters in the Co-MCM-41 pore may be smaller than the average estimated. The EXAFS data correlate well with the Raman characterization of the SWNT produced and confirms that small Co clusters are required for production of SWNT with good selectivity and a narrow diameter distribution.

4. Conclusions

A systematic investigation of the influence of the catalyst pretreatment and nanotube synthesis temperature on the characteristics of the SWNT diameter distribution produced in Co-MCM-41 was carried out. The results obtained by TGA, Raman spectroscopy, and HR-TEM, combined with EXAFS and XANES spectroscopy suggest that the diameter distribution and quality of SWNT in Co-MCM-41 can be engineered by controlling cobalt cluster size through the hydrogen prereduction and the reaction temperature. Cobalt in Co-MCM-41 becomes more active for SWNT growth after partial reduction by hydrogen. The catalysts that are excessively reduced prior to exposure to CO form SWNT with a wider diameter distribution. A narrow distribution of SWNT diameter can be achieved at an optimized prereduction and reaction temperature, i.e., prereduction at 500–600 °C and reaction at 750–800 °C. The control of cobalt cluster sizes in Co-MCM-41 is the key to SWNT diameter control. The Co^{2+} isomorphously substituted for silica in the MCM-41 framework is stable under severe reaction conditions, allowing slow reduction and nucleation of metallic clusters for production of large carbon yields at high reaction temperatures with high selectivity for SWNT and narrow tube diameter distribution.

Acknowledgments

We thank DARPA-DSO for the financial support for this project. Partial support for the synthesis of the MCM-41 catalysts and the use of the National Synchrotron Light Source at Brookhaven National Laboratory was obtained from DoE-BES. We are grateful to Sergei Bachilo and Bruce Weisman at Rice University for the fluorescence measurement.

References

[1] H.J. Dai, Acc. Chem. Res. 35 (2002) 1035.
[2] A. Huczko, Appl. Phys. A 74 (2002) 617.
[3] S.B. Sinnott, R. Andrews, Crit. Rev. Solid State Mater. Sci. 26 (2001) 145.
[4] R.R. Bacsa, C. Laurent, A. Peigney, W.S. Bacsa, T. Vaugien, A. Rousset, Chem. Phys. Lett. 323 (2000) 566.
[5] G.D. Li, Z.K. Tang, N. Wang, J.S. Chen, Carbon 40 (2002) 917.
[6] S.M. Bachilo, L. Balzano, J.E. Herrera, F. Pompeo, D.E. Resasco, R.B. Weisman, J. Am. Chem. Soc. 125 (2003) 11186.
[7] D. Ciuparu, Y. Chen, S. Lim, G.L. Haller, L. Pfefferle, J. Phys. Chem. B 108 (2004) 503.
[8] W.E. Alvarez, F. Pompeo, J.E. Herrera, L. Balzano, D.E. Resasco, Chem. Mater. 14 (2002) 1853.
[9] J.E. Herrera, L. Balzano, A. Borgna, W.E. Alvarez, D.E. Resasco, J. Catal. 204 (2001) 129.
[10] B. Kitiyanan, W.E. Alvarez, J.H. Harwell, D.E. Resasco, Chem. Phys. Lett. 317 (2000) 497.
[11] M. Sugano, A. Kasuya, K. Tohji, Y. Saito, Y. Nishina, Chem. Phys. Lett. 292 (1998) 575.
[12] H. Kuzmany, B. Burger, M. Hulman, J. Kurti, A.G. Rinzler, R.E. Smalley, EuroPhys. Lett. 44 (1998) 518.
[13] M.S. Dresselhaus, P.C. Eklund, Adv. Phys. 49 (2000) 705.

[14] C. Journet, W.K. Maser, P. Bernier, A. Loiseau, M.L. delaChapelle, S. Lefrant, P. Deniard, R. Lee, J.E. Fischer, Nature 388 (1997) 756.
[15] S. Lim, D. Ciuparu, C. Pak, F. Dobek, Y. Chen, D. Harding, L. Pfefferle, G. Haller, J. Phys. Chem. B 107 (2003) 11048.
[16] E.P. Barrett, L.G. Joyner, P.P. Halenda, J. Am. Chem. Soc. 73 (1951) 373.
[17] M.J. O'Connell, S.M. Bachilo, C.B. Huffman, V.C. Moore, M.S. Strano, E.H. Haroz, K.L. Rialon, P.J. Boul, W.H. Noon, C. Kittrell, J.P. Ma, R.H. Hauge, R.B. Weisman, R.E. Smalley, Science 297 (2002) 593.
[18] L. Alvarez, A. Righi, T. Guillard, S. Rols, E. Anglaret, D. Laplaze, J.L. Sauvajol, Chem. Phys. Lett. 316 (2000) 186.
[19] U.D. Venkateswaran, A.M. Rao, E. Richter, M. Menon, A. Rinzler, R.E. Smalley, P.C. Eklund, Phys. Rev. B 59 (1999) 10928.
[20] D. Kahn, J.P. Lu, Phys. Rev. B 60 (1999) 6535.
[21] A.G. Rinzler, J. Liu, H. Dai, P. Nikolaev, C.B. Huffman, F.J. Rodriguez-Macias, P.J. Boul, A.H. Lu, D. Heymann, D.T. Colbert, R.S. Lee, J.E. Fischer, A.M. Rao, P.C. Eklund, R.E. Smalley, Appl. Phys. A 67 (1998) 29.
[22] Z.J. Shi, Y.F. Lian, F.H. Liao, X.H. Zhou, Z.N. Gu, Y.G. Zhang, S. Iijima, Solid State Commun. 112 (1999) 35.
[23] J.E. Herrera, D.E. Resasco, Chem. Phys. Lett. 376 (2003) 302.
[24] E.A. Stern, M. Newville, B. Ravel, Y. Yacoby, D. Haskel, Phys. B 209 (1995) 117.
[25] S. Lim, D. Ciuparu, Y. Chen, Y. Yang, L. Pfefferle, G.L. Haller, J. Phys. Chem. B (2004), in press.
[26] W. Shi, J.K. Johnson, Phys. Rev. Lett. 91 (2003) art. no. 015504.
[27] D.E. Resasco, W.E. Alvarez, F. Pompeo, L. Balzano, J.E. Herrera, B. Kitiyanan, A. Borgna, J. Nanoparticle Res. 4 (2002) 131.
[28] W.E. Alvarez, B. Kitiyanan, A. Borgna, D.E. Resasco, Carbon 39 (2001) 547.
[29] M.K. Neylon, C.L. Marshall, A.J. Kropf, J. Am. Chem. Soc. 124 (2002) 5457.
[30] A.I. Frenkel, C.W. Hills, R.G. Nuzzo, J. Phys. Chem. B 105 (2001) 12689.
[31] A.L. Ankudinov, B. Ravel, J.J. Rehr, S.D. Conradson, Phys. Rev. B 58 (1998) 7565.
[32] J.M. Thomas, W.J. Thomos, Principels and Practice of Heterogeneous Catalysis, VCH, New York, 1997.
[33] I. Coulthard, T.K. Sham, Phys. Rev. Lett. 77 (1996) 4824.
[34] R.W.G. Wychoff, Crystal Structures, vol. 3, second ed., Interscience, New York, 1963, p. 78.
[35] L. Campbell, L. Hedin, J.J. Rehr, W. Bardyszewski, Phys. Rev. B 65 (2002).